Two-well terahertz quantum-cascade laser with direct intrawell-phonon depopulation

Sushil Kumar,[1,a)] Chun Wang I. Chan,[1] Qing Hu,[1] and John L. Reno[2]
[1]*Department of Electrical Engineering and Computer Science, Research Laboratory of Electronics, Massachusetts Institute of Technology, Cambridge, Massachusetts 02139, USA*
[2]*Sandia National Laboratories, Center of Integrated Nanotechnologies, MS 1303, Albuquerque, New Mexico 87185-1303, USA*

(Received 8 July 2009; accepted 15 September 2009; published online 8 October 2009)

We report the simplest quantum-cascade laser (QCL) to-date with only two quantum wells per QCL period, and at low temperatures, only three subband levels participate in electron transport. The lower laser level is directly depopulated via intrawell longitudinal-optical phonon scattering, which is in contrast with all the previously demonstrated terahertz QCLs, and maintains an ultrashort lower level lifetime under all operating bias and temperatures. Optical gain is due to a diagonal photon-assisted tunneling transition. Laser operation at 4.6 THz is obtained up to a heat-sink temperature of 121 K with a low-temperature threshold current density of 350 A/cm^2. Due to the simplicity of a two-well design, its electrical transport behavior could be analyzed in greater detail. A thermally activated carrier leakage due to higher-energy parasitic levels is speculated to be the most likely cause of a steep rise in the lasing threshold current density with temperature. © *2009 American Institute of Physics*. [doi:10.1063/1.3243459]

Terahertz quantum-cascade lasers[1] (QCLs) can be designed with short injector regions due to the requirement of smaller static electric bias fields as compared to the midinfrared QCLs. Designs with only single injector levels have recently been demonstrated with four-levels per period participating in electrical transport.[2,3] Extending in the direction of ever simpler structures, we now present a QCL design with only three levels per period as shown in Fig. 1 (a similar design has been independently reported recently[4]). A minimum of two wells per module are required to independently set E_{21}, the radiative energy E_{32}, and the radiative dipole matrix element z_{32}.[5,6] Even as the performance of terahertz QCLs has steadily improved, cryogenic cooling is still required for operation.[8] The highest operating temperatures (T_{max}) are obtained with the *resonant-phonon* designs[9,10] with $T_{max} \sim 186$ K for a design with a diagonal radiative transition[11] and $T_{max} \sim 225$ K for a vertical design but one that uses magnetic-field for additional carrier confinement.[12] In either of these cases, the nonradiative scattering time from the upper laser level u to the lower laser level l (τ_{ul}) is enhanced due to reduced e-LO phonon scattering. The lower-level depopulation in resonant-phonon designs occurs by a combination of resonant-tunneling[13] and e-LO phonon scattering, which makes it slower and prone to be affected by dephasing that becomes stronger with temperature.[14] The *intrawell-phonon* depopulation mechanism in Fig. 1 is fundamentally different since it always maintains a short lower-level lifetime, which is insensitive to dephasing caused by interface roughness and impurities. One of the main goals of the present design, therefore, was to simultaneously obtain a large τ_{ul} (by making the $u \rightarrow l$ radiative transition diagonal[11]) and a small τ_l (due to the fast intrawell-phonon depopulation) in order to obtain a better temperature performance.

Figure 1 shows the designed bandstructure at the $1'-3$ resonance bias. A small value of $z_{32} \sim 40$ Å was chosen to keep the $3 \rightarrow 2$ transition diagonal.[11] The following values are then calculated for the level lifetimes due to e-LO phonon scattering: $\tau_{31} \sim 3.7$ ps, $\tau_{32} \sim \tau_{32}^{LO} e^{(\hbar\omega_{LO}-E_{32})/k_B T_e} \sim 1.0 e^{(200/T_e)}$ ps, and $\tau_{21} \sim 0.2$ ps, where τ_{32}^{LO} is the raw scattering time when the upper-level electrons are sufficiently energetic to emit LO phonons and T_e is the upper-level electron temperature. The ratio τ_{ul}/τ_l for the present intrawell-phonon design is approximately four times larger than the resonant-phonon design in Ref. 11 and ~7.5 times larger than the one in Ref. 15 (calculated for a value of $T_e \sim 200$ K), which was the main motivation for the chosen design. The designed structure, labeled as TW246, was grown by molecular-beam epitaxy (wafer VB0227) to yield an 8 μm thick active region with 246 repeated periods, and was processed into metal-metal waveguides and experimentally characterized as outlined in Ref. 15. Figure 2 shows the

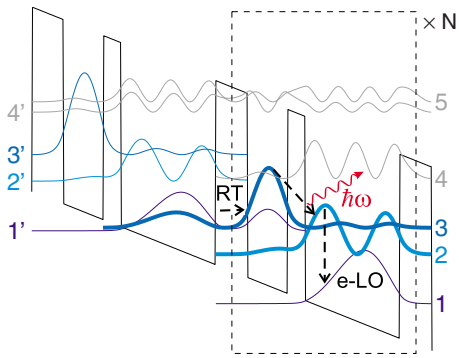

FIG. 1. (Color online) Conduction band diagram of the two-well (three-level) QCL design implemented in $GaAs/Al_{0.15}Ga_{0.85}As$. Electrons are injected into the upper laser level 3 from the injector $1'$ by resonant-tunneling. The optical gain is due to the $3 \rightarrow 2$ photon-assisted tunneling transition (Ref 7). The depopulation of the lower laser level 2 occurs directly by fast intrawell electron-longitudinal-optical (e-LO) phonon scattering back into the injector level 1 where $E_{21} \approx \hbar\omega_{LO}$. The layer thicknesses starting from the injector barrier in nm are 5.6/7.1/3.1/16.7. The injector well is uniformly n-doped to obtain an effective 2D density of 2.17×10^{10} cm^{-2} per period. At the design bias (17 kV/cm), $E_{21} \sim 37$ meV and $E_{32} \sim 19$ meV (4.6 THz).

a)Electronic mail: sushil@mit.edu.

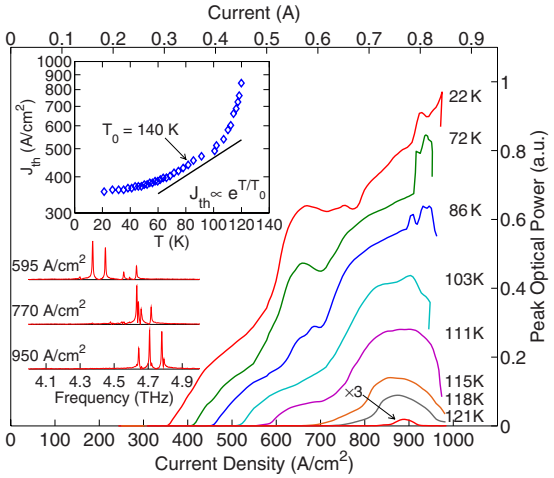

FIG. 2. (Color online) Pulsed (100 ns pulses repeated at 10 kHz) *L-I* characteristics from a 95 μm$\times$0.91 mm ridge laser. The top inset shows the variation of threshold current density J_{th} vs the heat-sink temperature T. The bottom inset shows representative spectra measured at 10 K.

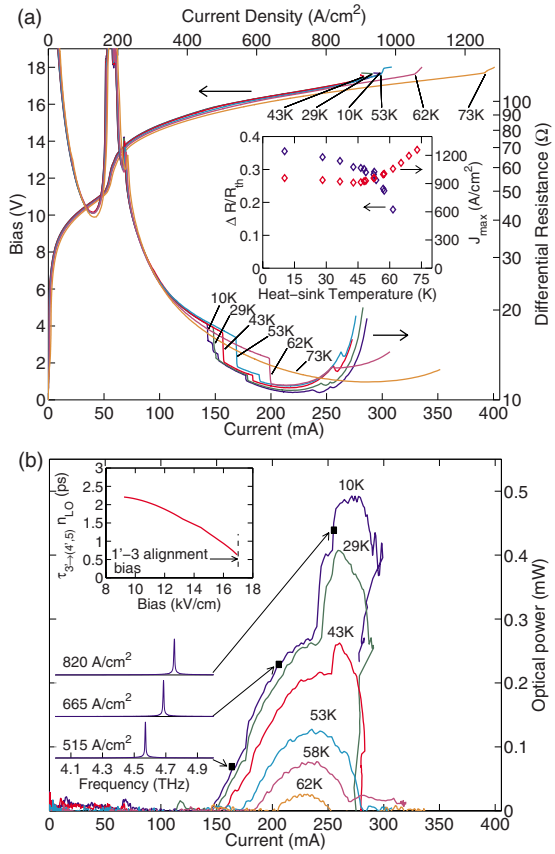

FIG. 3. (Color online) (a) cw *V-I* and $\mathcal{R}$-*I* measurements vs heat-sink temperature for a 20 μm$\times$1.56 mm ridge laser. The initial discontinuity in the $\mathcal{R}$-*I* curves marks the onset of lasing. Values of $T_{max,cw}\sim 63$ K and $T_{max,pul}\sim 104$ K were measured for this device suggesting a differential of $\sim$40 K between the heat-sink temperature and the lattice temperature. The inset shows temperature variation of the fractional discontinuity in R at threshold $[(\Delta\mathcal{R}_{th})/\mathcal{R}_{th}\equiv(\mathcal{R}_{th}^{-}-\mathcal{R}_{th}^{+})/\mathcal{R}_{th}^{-}]$ for the same device. $\mathcal{R}_{th}^{-}$ is the value of R just below threshold and $\mathcal{R}_{th}^{+}$ is taken as the value of R occurring immediately after a smaller second discontinuity that happens at $\sim$175 mA. Temperature variation of the peak current-density J_{max}, which is characterized by the discontinuity in the *I-V* at $\sim$17.5 V that occurs due to level misalignment beyond the $1'-3$ resonance, is also shown. (b) cw *L-I* for the same device (measured similarly as in Ref. 15). 10 K spectra at different points in the corresponding *L-I* are also shown. Every change in the lasing optical mode is accompanied by a change in the slope of the *L-I* (due to the changing beam shape), and also triggers a corresponding occurrence of a smaller discontinuity in the $\mathcal{R}$-*I* beyond the initial one. While the lasing mode changes with bias due to a Stark shifted gain spectrum, the reason for the corresponding (much smaller) change in the $\mathcal{R}$-*I* are not yet clear. Also note that the last $\mathcal{R}$-*I* discontinuity at $\sim$250 mA is not due to light turning off unlike that observed in Ref. 13. The upper inset shows calculated value of $\tau_{3'\rightarrow(4',5)}n_{LO}$ due to LO phonon scattering, where an electronic temperature of 200 K is assumed for the upper level population.

pulsed light-current (*L-I*) characteristics from a representative device that operated up to 121 K. Notwithstanding a lower threshold current density ($J_{th,10\ K}\sim 350$ A/cm^2) and a higher peak current density ($J_{max}\sim 950$ A/cm^2) at $T\sim 10$ K than the resonant-phonon QCLs in Refs. 11 and 15, the temperature performance for this intrawell-phonon QCL is significantly worse. A phenomenological fit to the expression $J_{th}\propto e^{T/T_0}$ that applies reasonably well to resonant-phonon QCLs is not applicable in the present case. While the low-temperature part of the $J_{th}-T$ curve can be fit approximately with a value $T_0\sim 140$ K typical of resonant-phonon designs,[6,11] J_{th} shows an unexpectedly stronger variation with temperature beyond $\sim$100 K as seen from Fig. 2 (inset).

The figure-of-merit parameters τ_{ul}/τ_l and $J_{max}/J_{th,10\ K}$ for the present design are better than the resonant-phonon designs in Refs. 11 and 15, and yet its T_{max} is significantly lower. In the following, we compare the present design with the 5-level resonant-phonon design of Ref. 15 to investigate possible reasons for this behavior. The active region in the resonant-phonon designs is spatially separated from the injector wells. As a consequence, the radiative levels have little spatial overlap with higher-energy parasitic levels that exist in the injector wells. However, as seen from Fig. 1, the upper radiative level ($3'$) of the present design has a significant spatial overlap with such parasitic levels ($4',5$).[6] We then attribute the poor temperature performance of this design to a thermally activated leakage from the upper radiative level to the aforementioned higher-energy parasitic levels. The energy separation between $3'-4',5$ is large ($E_{4'3'}\sim 36.5$ meV). Also, as will be shown next, there is evidence that any such $3'\rightarrow(4'5)$ scattering is thermally activated. For these two reasons, we speculate absorption of hot (non-equilibrium) LO phonons by upper-level electrons to be the most likely cause for such a leakage. A value of $\tau_{3'\rightarrow(4',5)}\sim n_{LO}^{-1}$ 0.55 ps is estimated for $T_e\sim 200$ K, where n_{LO} is the LO phonon occupation number in the active medium at the operating temperature. In comparison, $\tau_{u\rightarrow par}\sim n_{LO}^{-1}$ 4.6 ps for the resonant-phonon design in Ref. 15 (for the band diagram with parasitic levels, see Fig. 8 in Ref. 6), which is an order of magnitude slower. A non-negligible n_{LO} has been predicted for terahertz QCLs even at low temperatures due to the presence of hot LO phonons.[16] As a consequence, even a small non-equilibrium value of $n_{LO}\sim 0.1$ (for LO phonons in equilibrium with lattice, $n_{LO}^{eq}\sim 0.015$ at $T=100$ K) makes $\tau_3\sim 2.2$ ps, which is almost half of its low-temperature value ($\sim\tau_{31}\sim 3.7$ ps) and can degrade the laser performance considerably.

The thermally activated nature of the parasitic leakage channel becomes more clear after analyzing the continuous-wave (cw) voltage-current (*V-I*), differential-resistance-current ($\mathcal{R}$-*I*) and *L-I* characteristics from a narrower ridge laser as plotted in Fig. 3. The plateau in the *I-V* around $\sim$180 A/cm^2 is due to $1'-2$ alignment, which is considerably lower than the peak $J_{max}\sim 950$ A/cm^2 (as characterized by the negative-differential resistance discontinuity in the *I-V* occurring beyond the $1'-3$ resonance), and indicates

good $1' \rightarrow 3$ injection selectivity. The J_{max} for this device decreases slightly with the temperature T at $T < 45$ K, but then increases steeply again with T even while the device is still lasing. In contrast, the J_{max} for the resonant-phonon designs remains approximately constant up to the highest lasing temperature (for example, see Fig. 3 in Ref. 15). For lasing condition, the following expression can be derived for current flowing at the $1'-3$ resonance using a three-level density-matrix model and assuming a unity $1' \rightarrow 3$ injection efficiency[5,17]

$$J_{max} = en_{2D}\left[\frac{2\Omega_{1'3}^2\tau_{\parallel}\left(1-\Delta\mathcal{R}_{th}/\mathcal{R}_{th}\right)}{6\Omega_{1'3}^2\tau_{\parallel}\tau_{21}\tau_{31}/\left(\tau_{21}+\tau_{31}\right)+1}\right], \quad (1)$$

where, $\Delta\mathcal{R}_{th}/\mathcal{R}_{th}$ is the fractional discontinuity in the differential-resistance $\mathcal{R}$ that appears at the onset of lasing,[18,19] and is derived to be[5,17]

$$\frac{\Delta\mathcal{R}_{th}}{\mathcal{R}_{th}} \equiv \frac{\mathcal{R}_{th}^{-}-\mathcal{R}_{th}^{+}}{\mathcal{R}_{th}^{-}} = \frac{2\Delta n_{th}}{n_{2D}}\left[\frac{1-\tau_{21}/(2\tau_{31})}{1+\tau_{21}/\tau_{31}}\right] \quad (2)$$

Here, n_{2D} is the 2D doping density, Δn_{th} is the 2D population inversion density between level 3 and 2 at threshold, $2\hbar\Omega_{1'3}$ is the energy splitting at $1'-3$ anticrossing, and $\tau_{\parallel}$ is the dephasing time for $1' \rightarrow 3$ tunneling. From Eq. (1), J_{max} is independent of τ_{32} to a first order. It, however, depends sensitively on τ_{31} ($J_{max}\uparrow$ for $\tau_{31}\downarrow$). Note that these expressions are derived with a three-level model and may not be directly applicable to the structure in Fig. 1 once $3' \rightarrow (4',5)$ scattering becomes appreciable. However, any such scattered electrons eventually relax back into the injector level of a neighboring module in short time (the lifetimes $\tau_{4'} \sim \tau_5 \sim 0.3$ ps). Hence, such a channel can effectively be considered as a reduction in τ_{31}. With that assumption, Eq. (1) can describe J_{max} versus T behavior in Fig. 3(a) qualitatively. J_{max} changes only slightly up to $T \sim 43$ K (which is equivalent to a lattice temperature of 80–90 K), and then increases steeply at higher temperatures. This suggests that at low temperatures $T < 90$ K it is only τ_{32} that decreases with temperature (due to thermally activated $u \rightarrow l$ LO phonon emission akin to that for resonant-phonon QCLs). Subsequently, at higher temperatures, a reduction in τ_{31} dominates (due to the aforementioned $3' \rightarrow 4',5$ LO phonon absorption). Correspondingly, the measured $\Delta\mathcal{R}_{th}/\mathcal{R}_{th}$ deteriorates rapidly beyond $T \sim 45$ K, right when J_{max} starts to increase [see the Fig. 3(a) inset]. This is consistent with the interdependence of J_{max} and $\Delta\mathcal{R}_{th}/\mathcal{R}_{th}$ according to Eq. (1), and also the fact that $\Delta\mathcal{R}_{th}/\mathcal{R}_{th}$ depends sensitively on τ_{31} [$(\Delta\mathcal{R}_{th}/\mathcal{R}_{th})\downarrow$ as $\tau_{31}\downarrow$] according to Eq. (2). Also note that thermal backfilling from $1 \rightarrow 2$ is not likely to be the main cause for poor temperature performance of this design since an increase in τ_{21} should decrease J_{max} according to Eq. (1) contrary to the observed behavior.

Resonant-phonon QCLs typically emit maximum power at a bias close to the injector resonance, hence a maximum in the *L-I* coincides with J_{max} (see the *L-I* in Ref. 15). However, for the present design, the maximum of optical power occurs at a slightly lower current density, and for high temperature *L-I*, lasing even stops before the occurrence of J_{max} discontinuity as seen from Fig. 3(b). This is yet another evidence of a $3' \rightarrow 4',5$ scattering channel that becomes stronger at higher temperatures. As shown in the inset of Fig. 3(b), $\tau_{3' \rightarrow (4',5)}$ due to hot-phonon absorption decreases with bias (due to the decreasing $3'-4',5$ energy separation at higher bias when eventually $E_{4'3'} \approx \hbar\omega_{LO}$ at the $1'-3$ resonance bias). Consequently, the aforementioned leakage channel will reduce the gain close to the injector resonance if indeed a significant hot-phonon population n_{LO} exists.

While here we have presented the simplest QCL structure to date, a different depopulation mechanism was also demonstrated that maintains an ultrashort lower level lifetime under all operating conditions. The relatively poor temperature performance of this design compared to the resonant-phonon designs is attributed to thermally activated leakage due to higher-energy parasitic levels. Designs that could mitigate the role of such parasitic levels are likely to improve the temperature performance of terahertz QCLs.

This work is supported by AFOSR, NASA, and NSF. Sandia is a multiprogram laboratory operated by Sandia Corporation, a Lockheed Martin Co., for the U.S. Department of Energy under Contract No. DE-AC04–94AL85000.

[1] R. Köhler, A. Tredicucci, F. Beltram, H. E. Beere, E. H. Linfield, A. G. Davies, D. A. Ritchie, R. C. Iotti, and F. Rossi, Nature (London) **417**, 156 (2002).
[2] S. Kumar, B. S. Williams, Q. Hu, and J. L. Reno, Appl. Phys. Lett. **88**, 121123 (2006).
[3] H. Luo, S. R. Laframboise, Z. R. Wasilewski, G. C. Aers, H. C. Liu, and J. C. Cao, Appl. Phys. Lett. **90**, 041112 (2007).
[4] G. Scalari, M. I. Amanti, R. Terazzi, M. Beck, and J. Faist, Proceedings of the Tenth International Conference on Intersubband Transitions in Quantum Wells, Montreal, Canada, September 2009 (unpublished), http://www.itqw2009.com/index.php.
[5] S. Kumar, Ph.D. thesis, Massachusetts Institute of Technology, 2007.
[6] S. Kumar and A. W. M. Lee, IEEE J. Sel. Top. Quantum Electron. **14**, 333 (2008).
[7] R. F. Kazarinov and R. A. Suris, Sov. Phys. Semicond. **5**, 707 (1971).
[8] B. S. Williams, Nat. Photonics **1**, 517 (2007).
[9] B. S. Williams, H. Callebaut, S. Kumar, Q. Hu, and J. L. Reno, Appl. Phys. Lett. **82**, 1015 (2003).
[10] Q. Hu, B. S. Williams, S. Kumar, H. Callebaut, S. Kohen, and J. L. Reno, Semicond. Sci. Technol. **20**, S228 (2005).
[11] S. Kumar, Q. Hu, and J. L. Reno, Appl. Phys. Lett. **94**, 131105 (2009).
[12] A. Wade, G. Fedorov, D. Smirnov, S. Kumar, B. S. Williams, Q. Hu, and J. L. Reno, Nat. Photonics **3**, 41 (2009).
[13] G. Scalari, R. Terazzi, M. Giovannini, N. Hoyler, and J. Faist, Appl. Phys. Lett. **91**, 032103 (2007).
[14] R. Nelander and A. Wacker, Appl. Phys. Lett. **92**, 081102 (2008).
[15] B. S. Williams, S. Kumar, Q. Hu, and J. L. Reno, Opt. Express **13**, 3331 (2005).
[16] V. Spagnolo, M. S. Vitiello, G. Scamarcio, B. S. Williams, S. Kumar, Q. Hu, and J. L. Reno, J. Phys. Conf. Ser. **92**, 012018 (2007).
[17] S. Kumar and Q. Hu (unpublished).
[18] C. Sirtori, F. Capasso, J. Faist, A. L. Hutchinson, D. L. Sivco, and A. Y. Cho, IEEE J. Quantum Electron. **34**, 1722 (1998).
[19] L. Ajili, G. Scalari, J. Faist, H. Beere, E. Linfield, D. Ritchie, and G. Davies, Appl. Phys. Lett. **85**, 3986 (2004).